Quantum cascade laser based MIR spectrometer for the determination of CO and CO₂ concentrations and temperature in flames

Patrick Nau[1,2], Julia Koppmann[2], Alexander Lackner[2], Katharina Kohse-Höinghaus[2], Andreas Brockhinke[2]

[1] German Aerospace Center, Institute of Combustion Technology, Pfaffenwaldring 38–40, 70569 Stuttgart
[2] Universität Bielefeld, Physikalische Chemie 1, Universitätsstraße 25, 33615 Bielefeld

Abstract An experimental setup for the simultaneous detection of CO and CO_2 and the temperature in low-pressure flames using a pulsed quantum cascade laser (QCL) $4.48\,\mu m$ is presented. This comparatively new type of laser offers good output energies and beam quality in the mid-infrared (MIR), where the strong fundamental transitions of many molecules of interest can be accessed. A single-pass absorption setup was sufficient to obtain good accuracy for the stable species investigated here.

Due to the high repetition rate of the laser and the speed of the data acquisition, measurement of two-dimensional absorption spectra and subsequent tomographic reconstruction was feasible. As demonstration of this technique, two-dimensional CO and CO_2 concentrations have been measured in two fuel rich methane flames with different coflow gases (nitrogen and air). The influence of the coflow gas on the flame center concentration profiles was investigated and compared with 1D model simulations.

1 Introduction

Accurate measurements of species concentrations temperatures in flames are indispensable to characterize the combustion process and are a prerequisite for comparisons with numeric simulations. Laser diagnostics, being non-intrusive and non-destructive are an ideal choice for many flame applications. While many important radicals such as OH and CH have strong absorption bands in the UV/Vis and can easily be detected using techniques such as LIF or CRDS, electronic transitions of stable molecules like CO and CO_2 lie in the deep UV. Detection schemes like two-photon LIF[1] are possible, but quantification is prone to errors. For these molecules,

rovibrational transitions in the infrared provide an alternative detection method. Due to the availability of cheap tunable diode lasers in the near-infrared (NIR), this spectral region has already been widely used for combustion diagnostics in the past[2–5].

The strong fundamental bands in the mid-infrared (MIR) have the potential for a more sensitive detection compared to the weaker overtone bands in the NIR. The development of quantitative detection schemes in the MIR was, however, hindered by the lack of laser sources with adequate qualities. Most lasers available required cryogenic cooling and output powers were low[2, 6]. Wondraczek *et al.* used difference frequency generation (DFG) as an alternative method to generate MIR radiation. They detected CO around $5\,\mu m$ even though the output power of their laser system was only $30\,nW$[7]. In this work tomography has been applied to visualize CO in a flat flame.

In recent years, quantum cascade lasers (QCL) have proven to be reliable light sources in the MIR. Even though the operating principle for this type of laser has already been proposed in 1971 by Kazarinov and Suris[8], the first working quantum cascade laser has been presented more than twenty years later[9]. QCLs provide high output powers (several milliwatts) and narrow-band output with operation at room temperature which simplifies the experimental set up. This enables QCLs to compete with conventional techniques like fourier transform spectrometer for high resolution molecular spectroscopy in the infrared[10]. Application of a QCL for diagnostics in chemical vapor deposition processes[11] and flame exhaust gas diagnostics[12,13] have been presented before. Recently, temperature and concentration measurements of CO in shock tubes[14–16] and of combustion intermediates such as formaldehyde[17] have been performed as well.

In this contribution, we present simultaneous measurements of CO and CO_2 concentrations and flame temperatures with a QCL operating around $4.48\,\mu m$ ($2232\,cm^{-1}$) in laminar low-pressure flat flames. The

Correspondence to: Andreas Brockhinke, +49-521-106 2189, andreas.brockhinke@uni-bielefeld.de
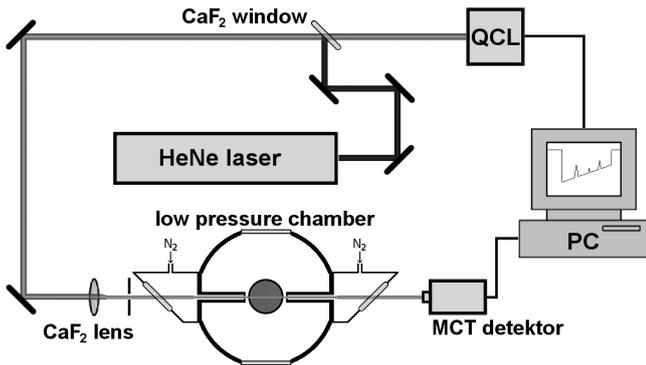
QCL has been operated in intra-pulsed spectroscopy mode[18]. In this mode the temperature induced frequency down-chirp is used to scan the laser over about $2\,cm^{-1}$ during the $500\,ns$ long laser pulses. Tomographic reconstruction has been applied to calculate the local absorption spectrum inside the flame. The spectra were used to obtain temperature and concentration with a least squares fitting algorithm. This way, 2D profiles for the temperature and concentration in the low-pressure flame have been obtained. In a second experiment, CO and CO_2 concentrations were measured in gas samples sampled from an atmospheric pressure flame. The rapid scanning of the QCL has been used to demonstrate the capability of the setup for single-pulse absorption measurements with repetition rates up to $100\,kHz$.

2 Experiment

The experimental setup for QCL absorption measurements in low-pressure flat flames is shown schematically in Fig. 1.

Laminar, premixed, flat fuel/oxygen/argon (25 % argon) flames have been stabilized on a home-made sintered bronze matrix burner. The diameter of the central matrix is $66\,mm$ diameter and is surrounded with a $20\,mm$ wide coflow matrix ring. This coflow helps to reduce absorption from the gas surrounding the flame. The burner can be moved vertically and horizontally with a stepper motor and is housed inside a vacuum chamber to stabilize the pressure at $50\,mbar$. Gas flows were regulated by calibrated mass flow controllers. The cold gas velocity at $300\,K$ for the fuel/oxygen mixture is $0.52\,m/s$.

The laser beam is focused into the center of the burner chamber with a CaF_2 lens ($f = +500\,mm$). A spatial resolution of $0.4\,mm$ in the burner center was measured with a knife edge technique. To reduce reflection losses and etaloning, both windows of the low-pressure chamber are arranged in Brewster's angle. Inside the chamber, the beam is guided through small tubes (inner diameter $5\,mm$) with a small exit hole (diameter $1\,mm$) towards the burner. A weak nitrogen
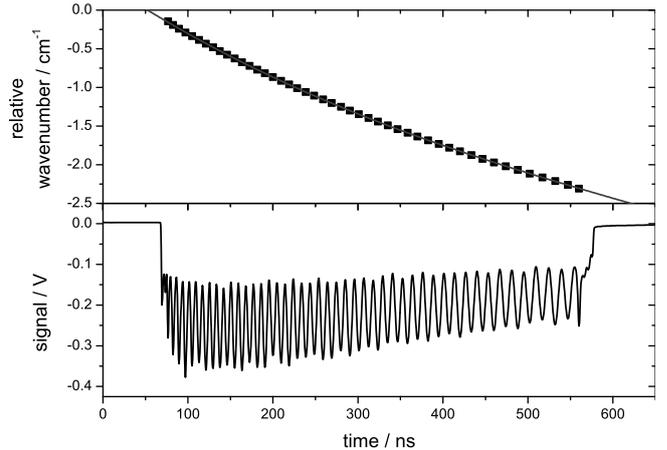
gas flow ($0.02\,slm$) prevents accumulation of combustion products in the tubes. Again, this reduces the influence from cold gas absorption. On the exit side of the burner chamber, the laser pulse is detected using a MCT detector (Vigo Systems, PVI-2TE-8) and digitized with a fast digitizer (Agilent-Acqiris, U1071A-002, 8 bit, $2\,GS/s$). The QCL (Cascade Technologies, LS-03-D, output power $0.7\,mW$) is operated in pulsed mode with a repetition frequency of $20\,kHz$ and a pulse length of $500\,ns$. The repetition rate was chosen to allow averaging of the signal to increase the signal-to-noise ratio significantly, but still keeping the duty cycle of the laser below the maximum value of $5\,\%$. Typically, 20,000 pulses are averaged. It should also be noted, that no influence of the repetition rate on the measured spectrum could be observed. The scanning speed of the laser is independent on the repetition rate, but only depends on the laser characteristics within the $500\,ns$ laser pulse. The base temperature of the laser head can be stabilized between $10\,°C$ and $30\,°C$.

A second flame experiment has been used for measurements in an absorption gas cell. An inverted V-shaped, premixed methane/air flame ($\phi = 0.85$, $10\,L/min$ total gas flow) is stabilized on a $60 \times 4\,mm$ sized slit burner at atmospheric pressure. In order to continuously extract gas samples, a $6\,mm$ diameter pipe is placed in the exhaust gas region above the slit flame. This gas sample flows through a $64\,cm$ long gas cell with a $1\,cm$ inner diameter. Thermocouples and a pressure sensor are connected to the cell to monitor temperature and pressure, respectively. Sample flow and pressure can be regulated with a rotary vane pump and needle valves. Wedged CaF_2 windows attached to each side of the gas cell serve as optical entrance and exit for the QCL laser pulses.

3 Data analysis and tomographic reconstruction

Intra-pulsed spectroscopy[18] has been used in this work. This has the advantage, that a complete absorption spectrum can be measured within a single laser pulse. Square current pulses with a relatively long width are used to drive the laser, which results in a considerable frequency down-chirp during each laser pulse. This way, the absorption spectrum is measured within only $500 \, \text{ns}$ measurement time. To quantify the temperature-induced frequency down-chirp, a germanium etalon (FSR = $0.048 \, \text{cm}^{-1}$) is placed in the beam path. The positions of the transmitted etalon signals have been fitted with a polynomial and have been used to calculate a relative wavenumber scale (Fig. 2). From this trace, the scanning speed is calculated to be about $120 \, \text{MHz/ns}$. This results in a linewidth of the laser of about $0.01 \, \text{cm}^{-1}$[19, 20]. During the $500 \, \text{ns}$ long laser pulses, the laser frequency is scanned over about $2 \, \text{cm}^{-1}$. The absolute wavenumber scale is obtained from the known line positions based on the HITRAN/HITEMP database[21, 22]. In the spectral range investigated here, the absorption lines of N_2O in a gas cell or, alternatively, those of the target molecules CO and CO_2, are well-suited for this purpose.

Absorption spectroscopy is described with Beer-Lambert's law. The measured absorption $\alpha_{\tilde{\nu}}$ at the given wavenumber $\tilde{\nu}$ is directly proportional to the absorption path length l and the number density N_m and absorption cross section $\sigma_m(T)$ of the molecule under investigation. The cross section at a given wavenumber depends on the integrated cross section $\sigma_m(T)$ with the temperature- and pressure-dependent line shape function $g(\tilde{\nu}, T, p)$. For gas mixtures, the measured absorption at a given wavenumber $\tilde{\nu}$ is the sum over all absorbing molecules m at this wavenumber.

$$\alpha_{\tilde{\nu}} = ln\frac{I}{I_0} = l \sum_m N_m \times \sigma_m(T) \times g(\tilde{\nu}, T, p) \quad (1)$$

In practice, the baseline of the absorption spectrum is taken from a laser pulse without absorbing species. From the natural logarithm of the ratio of absorption measurement (I) and baseline(I_0) the absorption spectrum is obtained. The baseline measurement was performed in the coflow region, without absorption from CO and CO_2.

Laminar flat flames are well-suited to study combustion chemistry, because of the nearly one-dimensional concentration and temperature in the flame center. In addition, they are very homogeneous (top hat geometry), which is a prerequisite for absorption spectroscopy. However, for stable species the flame edge and surrounding cold gas must be taken into account due to the line-of-sight character of absorption measurements. Because of the radial symmetry of the used flame, tomographic reconstruction can be easily applied. The absorption measurement is essentially an integration over different flame zones with radius r at a given distance of the laser beam from the flame center y

$$h(y) = 2 \int_y^R f(r) \frac{r}{\sqrt{r^2 - y^2}} \mathrm{d}r \quad (2)$$

The measured absorption for a given wavenumber is represented by $h(y)$, while $f(r)$ is the radial distribution of the absorption in the flame at the radius r. In this work we used the method of Dasch[23] for tomographic reconstruction. In this approach the deconvolution is calculated with a simple matrix multiplication:

$$f(y_i) = \frac{1}{\Delta y} \sum_{j=0}^{\infty} \mathbf{D}_{ij} h(y_j) \quad (3)$$

To reduce noise, the Three-Point Abel Deconvolution is used which uses a quadratic expansion around each point to act as a three-point smoothing operation. The operator $\mathbf{D}_{ij}$ is taken from Villarreal and Varghese[24]. Absorption spectra were measured with equally spaced $\Delta y = 1.5 \, \text{mm}$. This method allows a fast calculation of the radial distribution in the flame $f(y_i)$ from the measured projection data $h(y_i)$.

Similar to the method used by Villarreal and Varghese[24], complete absorption spectra were reconstructed, rather than the integrated radial absorption profiles of individual lines. This has the advantage that an absorption spectrum for every point inside the flame is obtained. A detailed discussion and description of the method can be found in [24]. These spectra were fitted with calculated spectra based on the HITEMP database[21]. Ren *et al.* showed that line strengths for CO in the HITEMP database are accurate to 2% even at flame temperatures[16]. Free parameters for the fitting process are temperature and concentrations of the molecules. The temperature-dependent Doppler linewidth is calculated for every molecule and is used in the fitting process. The algorithm is capable of fitting Voigt line shapes using the method for the calculation of the Voigt function of Humlicek[25]. Therefore, Doppler and pressure broadening can be considered, with Doppler broadening dominating in the low-pressure flame investigated here. In addition to the individual linewidths, the width of the laser due to the fast scanning frequency down chirp has been taken into account with a gaussian profile. With this procedure, temperature and concentrations of the molecules can be obtained at the same time for every point in the flame. The concentration is obtained from the absolute area under the spectral lines. In principle, it would be possible to infer a temperature from the measured linewidth. It is, however, much more accurate to determine the temperature using intensity ratios of different absorption lines in the measured spectra.
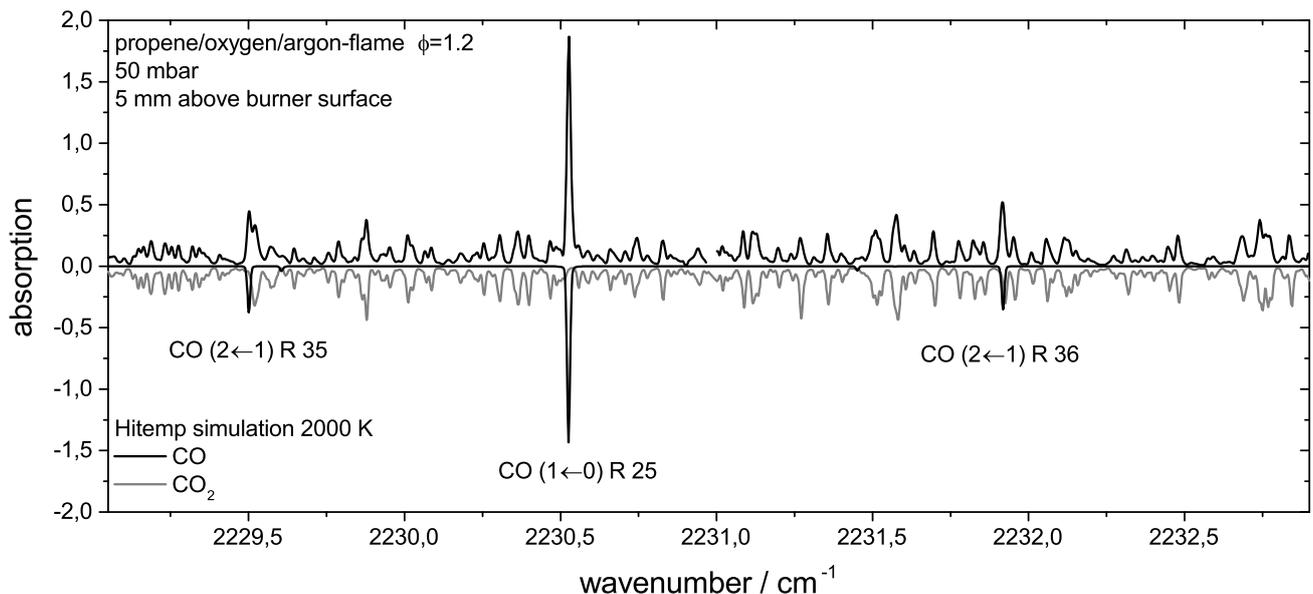
Fig. 3 Absorption spectrum of CO and CO_2 measured in a fuel rich propene flame at 50 mbar around 4.48 μm. The simulated spectra of both molecules are plotted on an inverted scale.

4 Results

The spectral range at 4.48 μm was chosen as it allows to detect both CO and CO_2. Figure 3 shows the absorption spectrum in a fuel-rich propene/oxygen-flame ($\phi = 1.2$, 50 mbar). To cover this range, two base temperatures of the laser head (12 °C and 27 °C) were used. A comparison with a simulated spectrum based on the HITEMP database[21] shows excellent agreement. Most of the lines can be assigned to the ν_4-band of CO_2. CO lines belong to the R-branch of the fundamental band. In addition to the strong $1 \leftarrow 0$ transition, lines from hot bands ($2 \leftarrow 1$ and $3 \leftarrow 2$) can be clearly identified as well. No interferences with other species are visible.

A measured and Abel-inverted absorption spectrum in a fuel rich methane/oxygen flame together with the fitted spectrum between 2231.4–2232.0 cm^{-1} is shown in Fig. 4 as an example. The agreement between measurement and fitted spectrum is very good. From the noise level in the Abel inverted spectrum, the minimum detectable absorption is determined to $1 \times 10^{-4}\,cm^{-1}$ at a measurement time of 1 s (20,000 averages). This corresponds to a lower detection limit for the CO mole fraction of 5.7×10^{-4} at 2100 K for the CO ($2 \leftarrow 1$) R 36 line in this spectral window. When the ($1 \leftarrow 0$) R 25 line is used, an even higher sensitivity could be achieved, especially at lower temperatures. Using that line, a minimum detectable mole fraction of 4.5×10^{-5} at 750 K and 1.6×10^{-4} at 2100 K would be attainable. It should, however, be noted that the actual lower detection limit for CO also depends on the CO_2 concentration due to the partial spectral overlap. This can limit the sensitivity, especially in lean flames. Due to the relatively high CO concentrations in the flames investigated here, sensi-
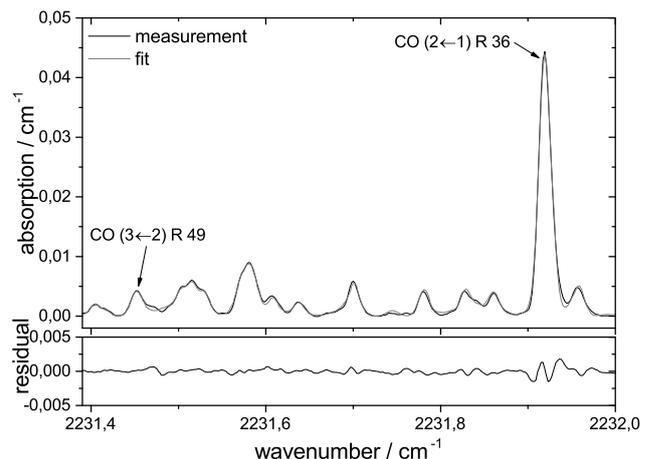

Fig. 4 Abel-inverted absorption spectrum of CO and CO_2 in a fuel rich ($\phi = 1.6$) methane/oxygen flame at 50 mbar and corresponding fit based on the constants from the HITEMP database. The two lines of CO in this region are marked with arrows; all remaining lines are due to CO_2.

tivity is not an issue. Therefore, using the hot band was a better choice (as it reduced undesired absorption from cold gas surrounding the flame).

To estimate the error in the measured concentration, several parameters have to be taken into account. The uncertainty for the intensity of the used CO lines is 2–5 % according to the HITEMP database. Furthermore, the uncertainty in the absorption cross section depends on the temperature dependence of the line $d\sigma/dT$ and the uncertainty in the measured temperature (5 %). The uncertainty in the obtained area of the absorption line from the fitting process including contributions from the tomographic reconstruction is estimated to about 5 %.
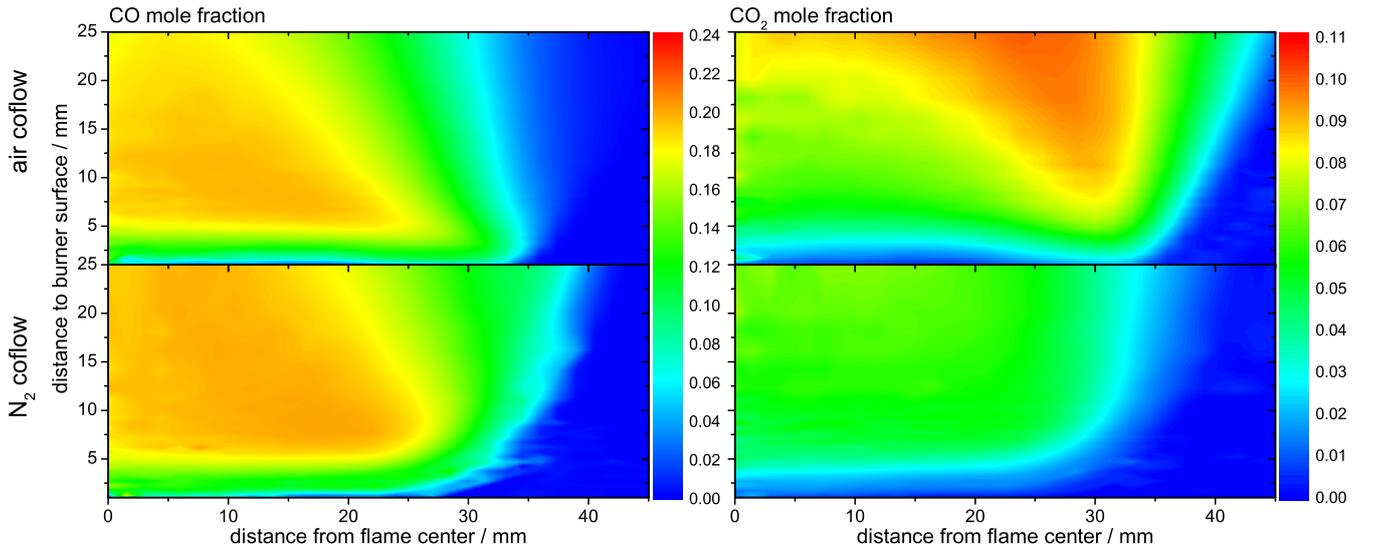
Fig. 5 Mole fraction maps of CO (left) and CO_2 (right) in the investigated fuel rich methane/oxygen ($\phi = 1.6$) flame with air (top) and N_2 (bottom) coflow gas.

These factors result in a total uncertainty of 9 % at the exhaust gas temperatures.

To study the influence of the coflow gas on the flame and demonstrate the capability of the system to determine two-dimensional concentration and temperature profiles, two different coflow gases have been used. Nitrogen and air were used with a cold gas velocity at 300 K of 1.21 m/s for the coflow. This shroud gas flow ensures a stable flame with zero absorption from CO and CO_2 in the coflow region. Zero absorption is advisable to guarantee a reliable Abel-inversion. Two dimensional concentration maps of CO and CO_2 are shown in Fig. 5 with different coflow gases. In both flames, the homogeneous region in the flame center decreases with increasing distance from the burner surface due to mixing with the surrounding gas. Especially at the flame edges, differences between both coflow gases are clearly visible.

For a more quantitative assessment of the influence of the different coflow gases, radial profiles of CO and CO_2 mole fractions as well as the temperature have been taken at three different heights above the burner surface (HAB = 5.7, 10.2 and 25.2 mm) and are shown in Fig. 6. Stable, plateau-like values for T, [CO] and [CO_2] are reached for HAB = 5.7 and 10.2 mm. This proves that the flames may in deed be treated as one-dimensional. For larger distances (HAB = 25.2 mm) this homogeneous zone becomes smaller, for even higher values it will vanish.

In the mixing layer between flame and coflow, a clear influence of the type of the coflow gas is observed. A diffusion flame is formed when air is used in the coflow. This can readily be seen at HAB = 5.7 mm by the increasing temperature, increasing CO_2 concentration and decreasing CO concentrations in the mixing layer. For larger HAB, the temperature differences in the mixing layer for the flame with air vs. that with N_2 coflow be-

come smaller. At radial positions smaller than 20 mm, the temperature is the same for all HAB, regardless of the coflow used. Larger deviations can be seen in the concentration fields when air is used as coflow: For larger HAB, diffusion effects lead to lower CO and higher CO_2 concentrations in a large area of the flame (essentially, the flame has a composition closer to stoichiometric). At HAB = 25.2 mm, even the centerline concentrations are affected.

For the flame with N_2 coflow the influence from the coflow gas seems altogether smaller, and the flame remains homogeneous in the center at significantly higher distances from the burner surface.

It is instructive to compare the measured flame center profiles with 1D model simulations, which are commonly used for this type of flames (see Fig. 7). Model simulations were calculated with the PREMIX package of ChemkinII and the GRI3.0 combustion mechanism[26]. To improve the signal-to-noise ratio in the height profiles, data points in the homogeneous flame center region were averaged. For the flame with N_2 coflow, this zone spanned a radius of 15 mm from the flame center, whereas averaging was only possible up to $r = 7.5$ mm for the flame with air coflow.

While there is almost no difference visible in the temperature profile for both flames, concentrations differ for CO and CO_2, especially at higher distances from the burner surface. When using air coflow, the CO concentration slightly decreases in the post flame front region while CO_2 concentration further increases. This is probably due to oxidation from surrounding air as mentioned above. In contrast, the CO concentration profile remains constant in the flame with N_2 coflow after reaching a maximum in the flame front. Comparison with model simulations using the GRI3.0 mechanism[26] shows very good agreement for the flame with N_2 coflow, while dif-
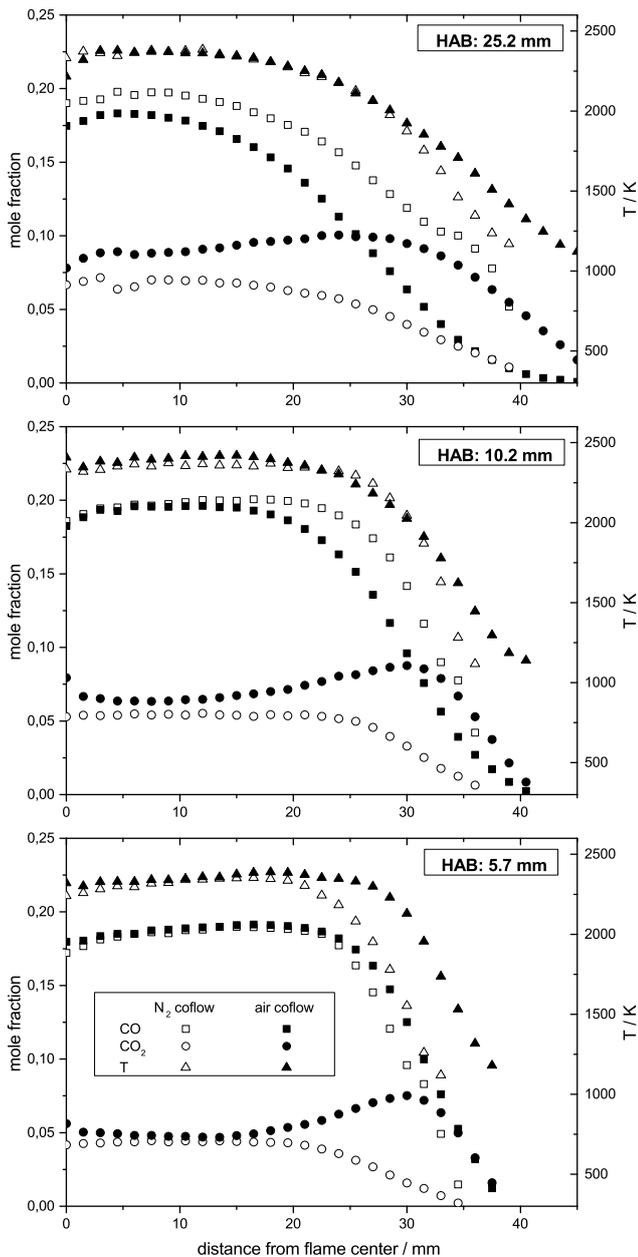
Fig. 7 Flame center mole fraction and temperature profiles in the investigated fuel rich methane/oxygen ($\phi = 1.6$) flame with different coflow gases. Model simulations were performed with ChemkinII and the GRI3.0 mechanism.

Fig. 6 Radial profiles of temperature, CO and CO_2 mole fractions for different heights above the burner (HAB) in a fuel rich methane/oxygen ($\phi = 1.6$) flame. Open symbols: With N_2 coflow. Closed symbols: With air coflow.

ferences can be observed for the flame with air coflow. It seems obvious that the simple 1D model is not sufficient to describe the flame for downstream positions larger than 15 mm, as influences from the surrounding coflow become significant.

To demonstrate the capability of the QCL laser setup for time-resolved measurements with high repetition rates an atmospheric pressure flame has been used. Gas samples were extracted from this flame and analyzed in an absorption cell (64 cm long) at 178 mbar. A single-pulse absorption spectrum as well as an absorp-
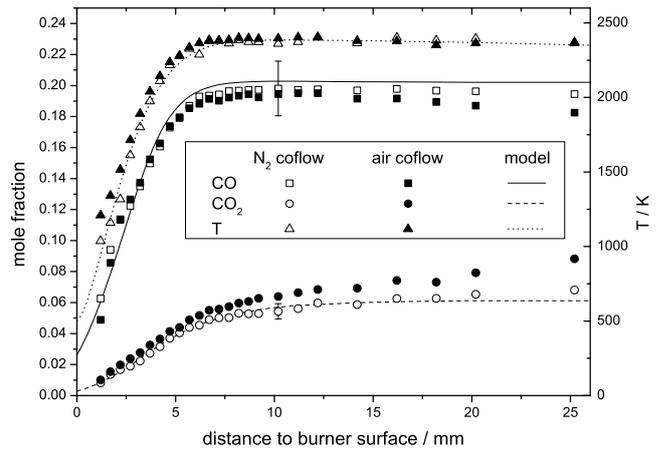
tion spectrum averaged over 10,000 laser pulses is shown in Fig. 8. In the investigated lean flame (ϕ=0.85) a CO concentration of 104 ppm has been measured. To determine the sensitivity the minimum detectable absorption was evaluated from the absorption spectra to 8×10^{-3} for the single-pulse measurement and 2×10^{-4} for 10,000 averages. This results in a lower detection limit for CO of 150 ppm and 4 ppm, respectively. Compared to measurements with a *cw* laser at a fixed wavelength[16], the rapid scanning of the QCL intra-pulsed spectroscopy offers the opportunity to measure complete absorption spectra with repetition rates up to 100 kHz. Additionally, intra-pulse spectroscopy allows straightforward detection and compensation of signal losses due to broadband absorption or scattering. It should be noted, that modern cw lasers in the MIR spectral range may be operated in a rapid-scanning mode as well (for cw DFB lasers in the NIR this option has already been available for a long time). For example, Ren *et al.* used a cw QCL modulated with 2.5 kHz for the detection of CO[16]. Continuous-wave interband cascade lasers (ICL) which have recently become available may be modulated with even higher frequencies. It is to be expected that these cw lasers will allow measurements with a better SNR. Pulsed lasers of the type we used here are, however, unique as they allow to measure a complete spectrum covering several cm^{-1} in a time of only a few hundreds of nanoseconds.

5 Conclusions

MIR absorption spectroscopy using a novel quantum cascade laser at $4.48\,\mu$m has been used to measure CO and CO_2 concentrations and flame temperatures in laminar premixed low-pressure flames. Tomographic reconstruction was used to take varying absorption along the line-of-sight into account and to obtain two-dimensional
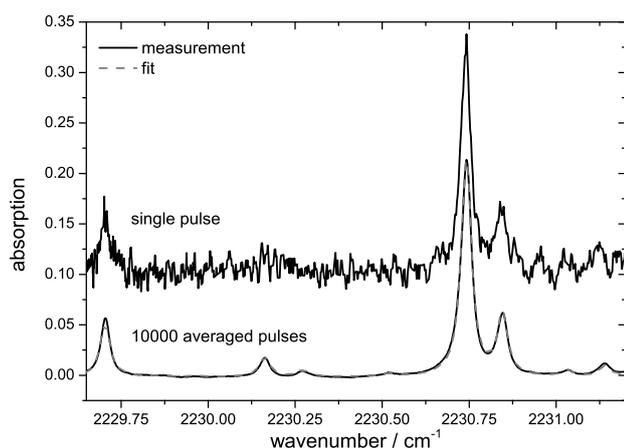
Fig. 8 Single-pulse and averaged absorption spectra together with the fitted spectrum. Measurements were performed in a gas cell at $178\,\text{mbar}$ and $294\,\text{K}$ at a laser repetition rate of $20\,\text{kHz}$. The single-pulse spectrum has been shifted for clarity.

concentration and temperature fields. Three-Point Abel Deconvolution has been used to determine complete absorption spectra at every point inside the flame. These spectra have been fitted using the spectral constants of the HITEMP database. A relative uncertainty of about $9\,\%$ is estimated for the measured concentrations under the flame conditions investigated.

Different coflow gases were used to study their influence on the concentration of stable species inside of the flame. Significant differences could be observed, especially for CO_2 concentrations. For the flame with air coflow, the CO_2 concentrations increases at the flame edge at higher distances from the burner surface, while CO concentrations decrease, due to oxidation of unburned fuel in the mixing region of flame and coflow gas. In contrast, this behavior can not be observed for the flame with N_2 coflow. At higher distances from the burner surface, the mixing region of flame and coflow gas gets wider. It has been shown that the coflow even affects concentration profiles at the flame center. Altogether, N_2 seems to be a better choice as a coflow gas. In this case, excellent agreement between simulated 1D profiles and measured concentrations has been achieved.

A singular advantage of the technique used is that the rapid scanning of the QCL allows to measure a complete absorption spectrum within a single laser pulse. During the $500\,\text{ns}$ long laser pulse used here, a spectral range of about $2\,\text{cm}^{-1}$ can be covered. This has been utilized for single-pulse measurements in a gas flow cell to analyze gas samples extracted from the exhaust gas region of an atmospheric-pressure flame. For single-pulse measurements, the lower detection limit of CO was about $150\,\text{ppm}$. The sensitivity can, however, easily been increased by averaging the absorption spectrum prior to data evaluation. Repetition rates up to $100\,\text{kHz}$ are possible with the laser used here, allowing time-resolved

measurements. This allows quantitative concentration measurements with high temporal resolution.

In summary, the QCL-based setup developed here certainly has merits for flame investigations − especially for quantitative measurements of stable species such as CO that can not be detected using single photon LIF.

References

1. M. Aldén, S. Wallin and W. Wendt, *Appl. Phys. B* **33** (1984), 205–208.
2. R. K. Hanson, P. A. Kuntz and C. H. Kruger, *Appl. Opt.* **16** (1977)(8), 2045–2048.
3. R. K. Hanson, *Proc. Combust. Inst.* **33** (2011), 1–40.
4. J. Wang, M. Maiorov, D. S. Baer, D. Z. Garbuzov, J. C. Connolly and R. K. Hanson, *Appl. Opt.* **39** (2000)(30), 5579–5589.
5. S. Wagner, M. Klein, T. Kathrotia, U. Riedel, T. Kissel, A. Dreizler and V. Ebert, *Appl. Phys. B* **109** (2012), 533–540.
6. K. L. McNesby, R. G. Daniel, J. B. Morris and A. W. Miziolek, *Appl. Opt.* **34** (1995)(18), 3318–3324.
7. L. Wondraczek, A. Khorsandi, U. Willer, G. Heide, W. Schade and G. H. Frischat, *Combust. Flame* **138** (2004)(1-2), 30–39.
8. R. F. Kazarinov and R. A. Suris, *Sov. Phys. Semicond.* **5** (1971), 707–709.
9. J. Faist, F. Capasso, D. L. Sivco, C. Sirtori, A. L. Hutchinson and A. Y. Cho, *Science* **264** (1994)(5158), 553–556.
10. G. Duxbury, D. Wilson, K. Hay and N. Langford, *J. Phys. Chem. A* **117** (2013), 9738–9745.
11. A. Cheesman, J. A. Smith, M. N. R. Ashfold, N. Langford, S. Wright and G. Duxbury, *J. Phys. Chem.* **A 110** (2006), 2821–2828.
12. S. D. Wehe, M. G. Allen, X. Liu, J. Jeffries and R. Hanson, NO and CO Absorption Measurements with a Mid-IR Quantum Cascade Laser for Engine Exhaust Applications, in *paper AIAA 2003-0588 at 41st Aerospace Sciences Meeting, Reno, NV* (Jan. 2003).
13. X. Chao, J.B. Jeffries and R.K. Hanson, *Proc. Combust. Inst.* (2012) **34**, 3583–3592.
14. J. Vanderover and M. A. Oehlschlaeger, *Appl. Phys. B* **99** (2010)(1-2), 353–362.
15. J. Vanderover, W. Wang and M. A. Oehlschlaeger, *Appl. Phys. B* **103** (2011)(4), 959–966.
16. W. Ren, A. Farooq, D. Davidson and R. Hanson, *Appl. Phys. B* **107** (2012), 849–860.
17. P. Nau, J. Koppmann, A. Lackner and A. Brockhinke, "Detection of formaldehyde in flames using UV and MIR absorption spectroscopy", accepted for publication in *Z. Phys. Chem.* (2014).
18. E. Normand, M. McCulloch, G. Duxbury and N. Langford, *Opt. Lett.* **28** (2003), 16–18.

19. M.T. McCulloch, E.L. Normand, N. Langford, G. Duxbury and D.A. Newnham, *J. Opt. Soc. Am. B* **20** (2003), 1761–1768.

20. T. Beyer, M. Braun, S. Hartwig and A. Lambrecht, *J. Appl. Phys.* **95** (2004), 4551–4554.

21. L. S. Rothman, I. E. Gordon, R. J. Barber, H. Dothe, R. R. Gamache, A. Goldman, V. Perevalov, S. A. Tashkun and J. Tennyson, *J. Quant. Spectrosc. and Rad. Transfer* **111** (2010), 2139–2150.

22. HITRAN, http://www.cfa.harvard.edu/HITRAN/ (2012).

23. C. J. Dasch, *Appl. Opt.* **31** (1992)(8), 1146–1152.

24. R. Villarreal and P. Varghese, *Appl. Opt.* **44** (2005)(31), 6786–6795.

25. J. Humlicek, *J. Quant. Spectrosc. Radiat. Transfer* **27** (1982)(4), 437–444.

26. G. P. Smith, D. M. Golden, M. Frenklach, N. W. Moriarty, B. Eiteneer, M. Goldenberg, C. T. Bowman, R. K. Hanson, S. Song, J. William C. Gardiner, V. V. Lissianski and Z. Qin, GRI-Mech 3.0, http://www.me.berkeley.edu/gri_mech (2000).